Voltage controlled inversion of magnetic anisotropy in a ferromagnetic thin film at room temperature

M Weiler[1,5]**, A Brandlmaier**[1]**, S Geprägs**[1]**, M Althammer**[1]**, M Opel**[1]**, C Bihler**[2]**, H Huebl**[2,4]**, M S Brandt**[2]**, R Gross**[1,3] **and S T B Goennenwein**[1,3]

[1] Walther-Meißner-Institut, Bayerische Akademie der Wissenschaften, 85748 Garching, Germany
[2] Walter Schottky Institut, Technische Universität München, 85748 Garching, Germany
[3] Physik-Department, Technische Universität München, 85748 Garching, Germany
E-mail: mathias.weiler@wmi.badw.de

Abstract. The control of magnetic properties by means of an electric field is an important aspect in magnetism and magnetoelectronics. We here utilize magnetoelastic coupling in ferromagnetic/piezoelectric hybrids to realize a voltage control of magnetization orientation at room temperature. The samples consist of polycrystalline nickel thin films evaporated onto piezoelectric actuators. The magnetic properties of these multifunctional hybrids are investigated at room temperature as a function of the voltage controlled stress exerted by the actuator on the Ni film. Ferromagnetic resonance spectroscopy shows that the magnetic easy axis in the Ni film plane is rotated by $90°$ upon changing the polarity of the voltage V_p applied to the actuator. In other words, the in-plane uniaxial magnetic anisotropy of the Ni film can be inverted via the application of an appropriate voltage V_p. Using superconducting quantum interference device (SQUID) magnetometry, the evolution of the magnetization vector is recorded as a function of V_p and of the external magnetic field. Changing V_p allows to reversibly adjust the magnetization orientation in the Ni film plane within a range of approximately $70°$. All magnetometry data can

[4] Present address: Australian Research Council Centre of Excellence for Quantum Computer Technology, School of Physics, the University of New South Wales, Sydney, NSW 2052, Australia.
[5] Author to whom any correspondence should be addressed.

be quantitatively understood in terms of the magnetic free energy determined from the ferromagnetic resonance experiments. These results demonstrate that magnetoelastic coupling in hybrid structures is indeed a viable option to control magnetization orientation in technologically relevant ferromagnetic thin films at room temperature.

Contents

1. Introduction

Multifunctional material systems unite different, e.g. electric and magnetic, functionalities in either a single phase or a heterostructure. They thus are of great fundamental and technological interest. Given that the electric and magnetic properties furthermore are coupled, it becomes possible to control either the magnetization by the application of an electric field or the electric polarization via a magnetic field alone. An electric field control of magnetization is particularly appealing, as it removes the need to generate magnetic fields of sufficient strength for magnetization switching on small length scales—thus enabling novel concepts for high density magnetic data storage applications. Thus, techniques to control the magnetization by means of electric fields or currents have recently been vigorously investigated and several schemes for an electric control of magnetization have been reported. These include the spin-torque effect [1]–[4] in spin-valves and magnetic tunnel junctions and the direct electric field control of magnetization in intrinsically multiferroic materials [5]–[12] or in ferromagnetic/ferroelectric heterostructures [13, 14]. A third, very attractive approach for the electric field control of magnetization takes advantage of the elastic channel, i.e. magnetostrictive coupling [15]–[23]. We here show that magnetoelasticity—that is the effect of lattice strain on magnetic anisotropy—in a polycrystalline nickel (Ni) film/piezoelectric actuator hybrid structure can be used to switch the magnetic easy axis in the Ni film by 90° at room temperature by simply changing the polarity of the voltage V_p applied to the actuator. The highly efficient coupling between piezoelectric and magnetic degrees of freedom in the ferromagnet/piezoactuator hybrid furthermore allows to achieve either an irreversible magnetization orientation control of 180° or a reversible control close to 90°, depending on whether the magnetization orientation is prepared in a local or global minimum of the free energy via a magnetic field sweep prior to the electric control experiment. We use ferromagnetic resonance (FMR) to quantify the effect of an electric field on magnetic anisotropy, which enables us to calculate the magnetization orientation as a function of V_p using a Stoner–Wohlfarth approach [24]. The magnetization orientation as a function of magnetic and electric fields determined in superconducting quantum interference device (SQUID)

magnetometry experiments is in full agreement with Stoner–Wohlfarth simulations, even for external magnetic field strengths well below the Ni coercive field. These experiments demonstrate that the strain-mediated electric field control of magnetization is indeed a viable technique in technologically relevant ferromagnetic thin films at room temperature.

2. Sample preparation and experimental techniques

We fabricated ferromagnetic thin film/piezoelectric actuator structures by depositing Ni thin films onto piezoelectric $Pb(Zr_xTi_{1-x})O_3$-based actuators [25]. Ni was chosen as the ferromagnetic constituent as it is a prototype 3d itinerant ferromagnet with a Curie temperature $T_c = 627$ K well above room temperature [26], a high bulk saturation magnetization $M_s = 411$ kA m^{-1} [27] and sizeable volume magnetostriction [28, 29] $\bar{\lambda} = \frac{2}{5}\lambda_{100} + \frac{3}{5}\lambda_{111} = -32.9 \times 10^{-6}$ with λ_{100} and λ_{111} being the single crystal saturation magnetostriction for a magnetic field applied along a crystalline $\langle 100 \rangle$ or $\langle 111 \rangle$ axis, respectively. The actuators exhibit a hysteretic mechanical stroke of up to 1.3×10^{-3} along their dominant elongation axis [cf figure 1(a)] if voltages -30 V $\leqslant V_p \leqslant +150$ V are applied. Prior to the deposition of the Ni film, the actuators were mechanically polished to a size of $x \times y \times z = 3 \times 2.6 \times 2$ mm^3 [cf figure 1(a)] to accommodate the size of the sample to the restrictions imposed by the FMR setup. We then used electron beam evaporation at a base pressure of 2.0×10^{-8} mbar to deposit a 70 nm thick Ni film onto an area of 5mm^2 on the $\hat{\mathbf{x}}$–$\hat{\mathbf{y}}$ face of the actuators. To prevent oxidation of the Ni film, a 10 nm thick Au film was deposited *in situ* on top of the Ni layer. The multifunctional hybrid obtained after Ni deposition is sketched schematically in figure 1(a) together with the definition of the angles that describe the orientation of the magnetization $\mathbf{M} = (M, \Theta, \Phi)$ and the external magnetic field $\mathbf{H} = (H, \theta, \phi)$ in the sample-affixed coordinate system.

To determine the static magnetic response of the ferromagnetic thin film/piezoelectric actuator hybrid we employ SQUID magnetometry. The Quantum Design MPMS-XL-7 SQUID magnetometer is sensitive to the projection $m = \mathbf{m}\hat{\mathbf{H}}$ of the total magnetic moment $\mathbf{m}$ onto the unit vector $\hat{\mathbf{H}} = \mathbf{H}/H$. We corrected m for the paramagnetic contribution of the actuator and used the Ni film volume $V = 3.5 \times 10^{-13}$ m^3 to calculate the respective projection $M = m/V$ of the magnetization onto $\hat{\mathbf{H}}$. All magnetometry data shown in the following were recorded at a temperature $T = 300$ K.

The magnetic anisotropy of the ferromagnetic thin film/piezoelectric actuator hybrid was measured by FMR at room temperature. We use a Bruker ESP 300 spin resonance spectrometer with a TE$_{102}$ cavity operating at a constant microwave frequency $\nu_{MW} = 9.3$ GHz. The sample can be rotated in the FMR setup with respect to the external dc magnetic field, so that either θ or ϕ [cf figure 1(a)] can be adjusted at will. To allow for lock-in detection we use magnetic field modulation at a modulation frequency of 100 kHz with a modulation amplitude of $\mu_0 H_{mod} = 3.2$ mT.

3. Phenomenology of strain-induced magnetic anisotropy

The piezoelectric actuator deforms upon the application of a voltage $V_p \neq 0$ V. Due to its elasticity, an elongation (contraction) along one Cartesian direction is always accompanied by a contraction (elongation) in the two orthogonal directions. Therefore, for $V_p > 0$ V, the actuator expands along its dominant elongation axis $\hat{\mathbf{y}}$ and contracts along the two orthogonal directions
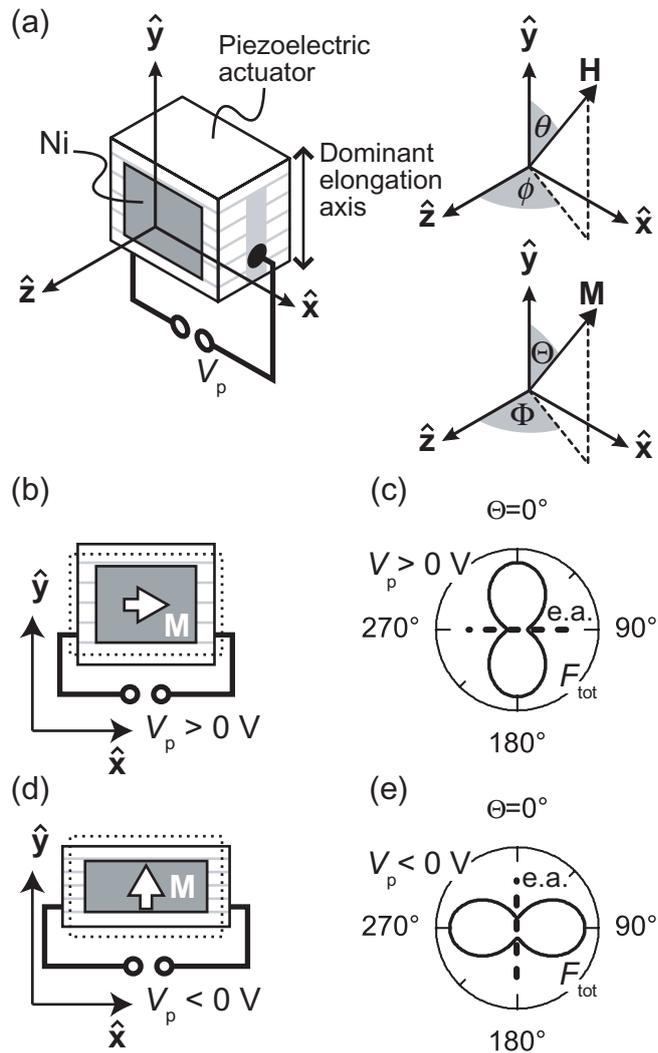
Figure 1. (a) Schematic illustration of the ferromagnetic thin film/piezoelectric actuator hybrid. (b) and (d) The application of a voltage $V_p \neq 0\,\text{V}$ to the actuator results in a deformation of the actuator and the affixed ferromagnetic film. The relaxed actuator at $V_p = 0\,\text{V}$ is shown by dotted contours. (c) and (e) Schematic free energy contours in the film plane. The magnetic easy axis (e.a.) shown by the thick dashed line is oriented parallel to the compressive strain and can thus be rotated by $90°$ by changing the polarity of V_p.

$\hat{\mathbf{x}}$ and $\hat{\mathbf{z}}$. The Ni film affixed to the $\hat{\mathbf{x}}$–$\hat{\mathbf{y}}$ face of the actuator is hence strained tensilely along $\hat{\mathbf{y}}$ and compressively along $\hat{\mathbf{x}}$ for $V_p > 0\,\text{V}$ [cf figure 1(b)]. For $V_p < 0\,\text{V}$ the actuator contracts along $\hat{\mathbf{y}}$ and thus expands along $\hat{\mathbf{x}}$ and $\hat{\mathbf{z}}$ and the Ni film thus exhibits a compressive strain along $\hat{\mathbf{y}}$ and a tensile strain along $\hat{\mathbf{x}}$ [cf figure 1(d)].

To describe the impact of this lattice strain on the Ni magnetization orientation we use a magnetic free energy density approach. The free energy F_{tot} is a measure for the angular dependence of the magnetic hardness, with maxima in F_{tot} corresponding to magnetically hard directions and minima to magnetically easy directions. In equilibrium, the magnetization always

resides in a local minimum of F_{tot}. Contrary to single-crystalline films, the evaporated Ni films are polycrystalline and thus show no net crystalline magnetic anisotropy which may compete with strain-induced anisotropies and hereby reduce the achievable magnetization orientation effect [19]. F_{tot} is thus given by

$$F_{tot} = F_{stat} + F_{demag} + F_{magel}. \tag{1}$$

The first term $F_{stat} = -\mu_0 M H (\sin\Theta \sin\Phi \sin\theta \sin\phi + \cos\Theta \cos\theta + \sin\Theta \cos\Phi \sin\theta \cos\phi)$ in equation (1) is the Zeemann term and describes the influence of an external magnetic field **H** on the orientation of **M**. The uniaxial demagnetization term $F_{demag} = (\mu_0/2) M^2 \sin^2\Theta \cos^2\Phi$ is the anisotropy caused by the thin-film shape of the sample [30]. The last contribution to equation (1)

$$\begin{aligned} F_{magel} = \tfrac{3}{2}\bar{\lambda}\left(c_{12}^{Ni} - c_{11}^{Ni}\right)\big[&\varepsilon_1(\sin^2\Theta \sin^2\Phi - 1/3) \\ &+ \varepsilon_2(\cos^2\Theta - 1/3) + \varepsilon_3(\sin^2\Theta \cos^2\Phi - 1/3)\big] \end{aligned} \tag{2}$$

describes the influence of the lattice strains on the magnetic anisotropy [28]. The strains along the $\hat{\mathbf{x}}$-, $\hat{\mathbf{y}}$- and $\hat{\mathbf{z}}$-axis are denoted in Voigt (matrix) notation [31] as $\varepsilon_1, \varepsilon_2$ and ε_3, respectively. Furthermore, $c_{11}^{Ni} = 2.5 \times 10^{11}\,\mathrm{N\,m^{-2}}$ and $c_{12}^{Ni} = 1.6 \times 10^{11}\,\mathrm{N\,m^{-2}}$ are the elastic moduli of Ni [29]. The effects of shear strains (ε_i, $i \in \{4, 5, 6\}$) average out in our polycrystalline film and thus are neglected.

Using $\sin^2\Theta \sin^2\Phi + \cos^2\Theta + \sin^2\Theta \cos^2\Phi = 1$ and omitting isotropic terms, equation (2) can be rewritten as

$$F_{magel} = K_{u,magel,y}\cos^2\Theta + K_{u,magel,z}\sin^2\Theta \cos^2\Phi \tag{3}$$

with

$$\begin{aligned} K_{u,magel,y} &= \tfrac{3}{2}\bar{\lambda}\left(c_{12}^{Ni} - c_{11}^{Ni}\right)(\varepsilon_2 - \varepsilon_1), \\ K_{u,magel,z} &= \tfrac{3}{2}\bar{\lambda}\left(c_{12}^{Ni} - c_{11}^{Ni}\right)(\varepsilon_3 - \varepsilon_1). \end{aligned} \tag{4}$$

Due to the elasticity of the actuator and the Ni film, the strains ε_i are not independent of each other. The strains ε_1 and ε_2 in the $\hat{\mathbf{x}}$–$\hat{\mathbf{y}}$-plane are linked by the Poisson ratio $\nu = 0.45$ of the actuator [25] according to

$$\varepsilon_1 = -\nu\varepsilon_2. \tag{5}$$

Furthermore, due to the elasticity of the Ni film, the out-of-plane strain ε_3 can be expressed as [19]

$$\varepsilon_3 = -\frac{c_{12}^{Ni}}{c_{11}^{Ni}}(\varepsilon_1 + \varepsilon_2). \tag{6}$$

Assuming a linear expansion of the actuator with lateral dimension L parallel to its dominant elongation axis, we can calculate the strain in the Ni film parallel to the actuator's dominant elongation axis as

$$\varepsilon_2 = \frac{\delta L}{L}\frac{V_p}{180\,\mathrm{V}}, \tag{7}$$

where $\delta L/L = 1.3 \times 10^{-3}$ is the nominal full actuator stroke for the full voltage swing $-30\,\mathrm{V} \leqslant V_p \leqslant +150\,\mathrm{V}$. With equations (5)–(7) all strains in the Ni film can thus directly be calculated for any given voltage V_p. This allows to determine the equilibrium orientation of the magnetization as a function of V_p by minimizing the total magnetoelastic free energy density F_{tot} [equation (1)].

Due to the negative magnetostriction ($\bar{\lambda} < 0$) of Ni and $c_{11}^{Ni} > c_{12}^{Ni}$, the in-plane easy axis of F_{tot} is oriented orthogonal to tensile and parallel to compressive strains in the absence of external magnetic fields. Due to the strong uniaxial out-of-plane anisotropy caused by F_{demag}, the in-plane easy axis is the global easy axis. For $V_p > 0$ V, the Ni film exhibits a tensile strain along $\hat{\mathbf{y}}$ ($\varepsilon_2 > 0$) and a compressive strain along $\hat{\mathbf{x}}$ ($\varepsilon_1 < 0$). The easy axis of F_{tot} is thus oriented along the $\hat{\mathbf{x}}$-direction [cf figure 1(c)]. Accordingly, for $V_p < 0$ V, the easy axis of F_{tot} is oriented parallel to the compressive strain along $\hat{\mathbf{y}}$ and orthogonal to the tensile strain along $\hat{\mathbf{x}}$ [cf figure 1(e)]. We thus expect a 90° rotation of the in-plane easy axis of F_{tot} upon changing the polarity of V_p. Note that in the absence of external magnetic fields there are always two energetically equivalent antiparallel orientations of **M** along the magnetic easy axis. However, for simplicity, we only show one of the two resulting possible in-plane orientations of **M** in figures 1(b) and (d). Nevertheless, these panels show that it should be possible to change the orientation of **M** from **M**∥$\hat{\mathbf{x}}$ to **M**∥$\hat{\mathbf{y}}$ via the application of appropriate voltages V_p to the actuator.

The total magnetic free energy density F_{tot} in equation (1) is experimentally accessible by FMR. The FMR equations of motion [32]–[34]

$$\left(\frac{\omega}{\gamma}\right)^2 = \frac{1}{M_s^2 \sin^2 \Theta}\left(\left(\partial_\Phi^2 F_{tot}\right)\left(\partial_\Theta^2 F_{tot}\right) - \left(\partial_\Phi \partial_\Theta F_{tot}\right)^2\right)\big|_{\Theta_0, \Phi_0} \tag{8}$$

and

$$\partial_\Theta F_{tot}|_{\Theta=\Theta_0} = \partial_\Phi F_{tot}|_{\Phi=\Phi_0} = 0$$

link the experimentally determined FMR field $\mu_0 H_{res}$ to the magnetic free energy density F_{tot}. In equation (8), γ is the gyromagnetic ratio and $\omega = 2\pi \nu_{MW}$ with the microwave frequency ν_{MW}. The effect of damping is neglected in equation (8), as damping only affects the lineshape which will not be discussed in this article. We note that the FMR resonance field $\mu_0 H_{res}$ measured in experiment can be considered as a direct indicator of the relative magnetic hardness along the external dc magnetic field direction. From equations (1) and (8) one finds that smaller resonance fields correspond to magnetically easier directions and larger resonance fields to magnetically harder directions.

4. FMR

In this section, we quantitatively determine the magnetic anisotropy of our ferromagnetic thin film/piezoelectric actuator hybrid structure using FMR measurements. Figure 2(a) shows four FMR spectra recorded at room temperature with **H**∥$\hat{\mathbf{y}}$ and a voltage $V_p \in \{-30\,\text{V}, 0\,\text{V}, 30\,\text{V}, 90\,\text{V}\}$ applied to the actuator, respectively. Each spectrum shows one strong FMR which—due to the magnetic field modulation and lock-in detection—has a lineshape corresponding to the first derivative of a Lorentzian line [35]. The resonance field $\mu_0 H_{res}$ of a given FMR line is determined as the arithmetic mean of its maximum and minimum and depicted by the full squares in figure 2(a). The figure shows that, with the external magnetic field **H**∥$\hat{\mathbf{y}}$, $\mu_0 H_{res}$ is shifted to higher magnetic fields for increasing V_p, while the lineshape is not significantly changed. According to equations (1) and (8), this implies that the $\hat{\mathbf{y}}$-direction becomes increasingly harder as V_p is increased.

To determine the evolution of $\mu_0 H_{res}$ with V_p in more detail, we recorded FMR spectra similar to those shown in figure 2(a) for V_p increasing from -30 V to $+90$ V (upsweep) and decreasing back to -30 V (downsweep) in steps of $\Delta V_p = 10$ V. For **H**∥$\hat{\mathbf{y}}$, we obtain the
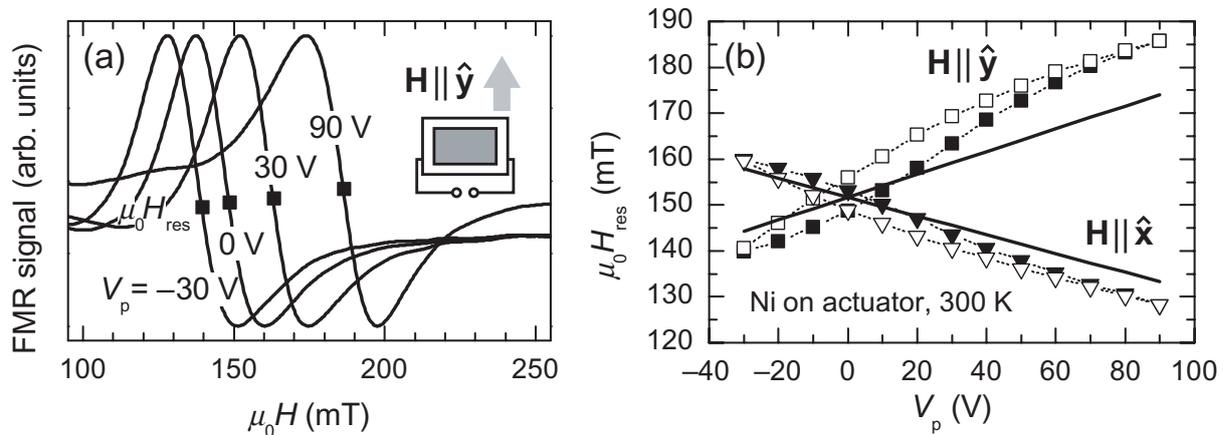
Figure 2. (a) FMR spectra recorded with $\mathbf{H} \| \hat{\mathbf{y}}$ at different voltages V_p. An increasing resonance field $\mu_0 H_{res}$ (solid squares) is observed for increasing V_p while the lineshape is not significantly altered. (b) The dependence of $\mu_0 H_{res}$ on V_p is qualitatively different for $\mathbf{H} \| \hat{\mathbf{y}}$ and $\mathbf{H} \| \hat{\mathbf{x}}$. Full symbols correspond to increasing V_p and open symbols to decreasing V_p. The solid lines represent the resonance fields calculated from magnetoelastic theory (cf section 3) yielding very good agreement with the measurement. For $\mathbf{H} \| \hat{\mathbf{y}}$, increasing V_p increases $\mu_0 H_{res}$ and thus the magnetic hardness of this direction, while for $\mathbf{H} \| \hat{\mathbf{x}}$, increasing V_p decreases $\mu_0 H_{res}$ and thus the magnetic hardness of this direction. The hysteresis of $\mu_0 H_{res}$ is due to the hysteretic voltage–strain curve of the actuator.

resonance fields shown by the squares in figure 2(b). Here, full squares depict the upsweep and open squares the downsweep of V_p. As discussed in the context of figure 2(a), figure 2(b) shows that the FMR resonance field for $\mathbf{H} \| \hat{\mathbf{y}}$ increases with increasing V_p and decreases with decreasing V_p. The small hysteresis between up- and down-sweep is due to the hysteretic expansion of the actuator [25]. Carrying out the same series of FMR measurements with $\mathbf{H} \| \hat{\mathbf{x}}$ yields the resonance fields shown by the triangles in figure 2(b). For this magnetic field orientation, $\mu_0 H_{res}$ decreases for increasing V_p and vice versa. In terms of magnetic anisotropy we thus can conclude that the $\hat{\mathbf{x}}$-direction becomes easier for increasing V_p while at the same time the $\hat{\mathbf{y}}$-direction simultaneously becomes harder.

For a more quantitative discussion we have also plotted the behaviour expected from equations (1) and (8) as solid lines in figure 2(b). These lines show the resonance fields obtained by assuming a linear, non-hysteretic voltage–strain relation [cf equation (7)] and solving equation (8) with F_{tot} from equation (1). We use a saturation magnetization $M_s = 370 \, \mathrm{kA \, m^{-1}}$, as determined by SQUID measurements and a g-factor of 2.165 [36]. Considering the fact that the actuator expansion saturates at high voltages and the data in figure 2(b) only show a minor loop of the full actuator swing, the simulation is in full agreement to the experimental results. This demonstrates that for $V_p < 0 \, \mathrm{V}$ the $\hat{\mathbf{y}}$-direction is magnetically easier than the $\hat{\mathbf{x}}$-direction, while for $V_p > 0 \, \mathrm{V}$ the $\hat{\mathbf{x}}$-direction is easier than the $\hat{\mathbf{y}}$-direction. Moreover, at $V_p = 0 \, \mathrm{V}$, both measurement and simulation yield resonance fields of $\mu_0 H_{res} \approx 150 \, \mathrm{mT}$ for $\mathbf{H} \| \hat{\mathbf{y}}$ as well as $\mathbf{H} \| \hat{\mathbf{x}}$. Thus, at this voltage, both orientations $\hat{\mathbf{x}}$ and $\hat{\mathbf{y}}$ are equally easy in our sample.

To quantitatively determine the full magnetic anisotropy as a function of V_p, we recorded FMR traces at constant V_p for several different $\mathbf{H}$ orientations. The FMR resonance fields
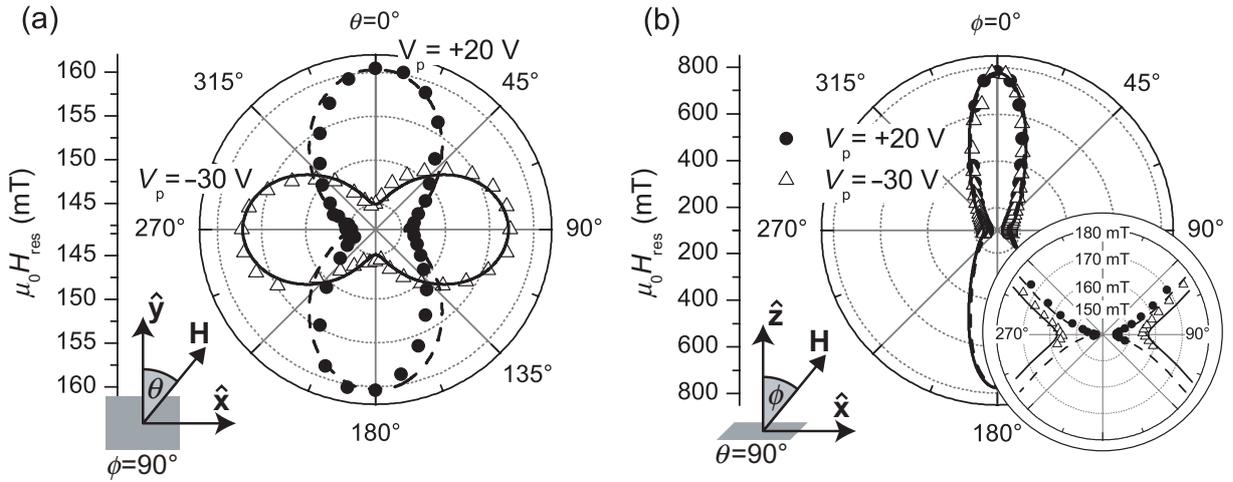
Figure 3. (a) The symbols show the FMR resonance field $\mu_0 H_{res}(\theta)$ obtained for a constant actuator voltage $V_p = -30\,V$ (open triangles) and $V_p = +20\,V$ (solid circles) as a function of the orientation θ of **H** in the sample plane. A uniaxial (180° periodic) anisotropy of $\mu_0 H_{res}(\theta)$ is observed for both voltages. However, the easy axis is rotated by 90° as V_p is changed from $+20\,V$ to $-30\,V$. The lines show the resonance fields simulated using the anisotropy constants from equation (9). (b) Corresponding experiments with **H** rotated in the $\hat{y}$-plane (from within the Ni film plane to out-of-plane). Regardless of V_p, a strong uniaxial anisotropy with the hard axis perpendicular to the film plane is observed. The inset shows that the resonance fields for **H** in the film plane ($\phi = 90°$ and $\phi = 270°$) are still shifted as a function of V_p in accordance to the data shown in (a) for $\theta = 90°$ and $\theta = 270°$.

thus determined in experiment are shown in figure 3 together with simulations according to equations (1) and (8). The open triangles in figure 3 represent the resonance fields obtained for $V_p = -30\,V$ and the full circles those obtained for $V_p = +20\,V$. Note that in the polar plots in figure 3, the distance of $\mu_0 H_{res}$ from the coordinate origin is an indicator of the magnetic hardness, with easy directions corresponding to small distances and hard directions to large distances.

If **H** is rotated in the film plane [cf figure 3(a), $\phi = 90°$], the obtained $\mu_0 H_{res}(\theta)$ shows minima at $\theta = 0°$ and $\theta = 180°$ for $V_p = -30\,V$ and at $\theta = 90°$ and $\theta = 270°$ for $V_p = +20\,V$, respectively. Thus, a clear 180° periodicity of the resonance fields and hence a uniaxial magnetic anisotropy is observed for both V_p. As the orientations θ corresponding to minima of $\mu_0 H_{res}$ for one voltage coincide with maxima for the other voltage, we conclude that the direction of the easy axis is rotated by 90° if V_p is changed from $V_p = -30\,V$ to $V_p = +20V$. This is exactly the behaviour expected according to figures 1(c) and (e).

If **H** is rotated from within the film plane ($\phi = 90°$, $\theta = 90°$) to perpendicular to the film plane ($\phi = 0°$, $\theta = 90°$), we obtain the resonance fields shown in figure 3(b). In this case, we observe a strong uniaxial anisotropy with a hard axis perpendicular to the film plane regardless of V_p, stemming from the V_p-independent contribution F_{demag} to F_{tot}. The inset in figure 3(b) shows that for **H** in the film plane, the resonance fields for $V_p = -30\,V$ and $V_p = +20\,V$ are shifted by approximately 10 mT in full accordance to the data in figure 3(a).

As discussed in section 3, the V_p dependence of the resonance field is given by a V_p dependence of F_{magel}. We thus evaluate the measurement data shown in figures 3(a) and (b) using an iterative fitting procedure of $K_{u,magel,y}$ in equation (1) to fulfill equation (8). We obtain

$$K_{u,magel,y}(-30\,\text{V})/M_s = -3.4\,\text{mT}$$
$$K_{u,magel,y}(+20\,\text{V})/M_s = 4.4\,\text{mT}. \tag{9}$$

The resonance fields calculated using these anisotropy fields as well as equations (8) and (1) are depicted by the lines in figure 3. The good agreement between simulation and experiment shows that F_{tot} given by equation (1) is sufficient to describe the magnetic anisotropy of the Ni film.

In summary, the FMR experiments conclusively demonstrate that it is possible to invert the in-plane magnetic anisotropy of our hybrid structure, i.e. to invert the sign of $K_{u,magel,y}$ *solely by changing V_p*. As the FMR experiment furthermore allows to quantitatively determine all contributions to the free energy, equation (1), the orientation of the magnetization vector **M** in our sample can be calculated *a priori* for arbitrary **H** and V_p. However, it is not possible to directly measure the magnetization orientation as a function of V_p with FMR. To demonstrate that the piezo-voltage control of magnetic anisotropy indeed allows for a voltage control of **M**, we now turn to magnetometry.

5. Magnetometry

In this section, we show that it is possible to not only change the magnetic anisotropy but to deliberately *irreversibly* and/or *reversibly* rotate **M** simply by changing V_p. To this end, we need to employ an experimental technique that is directly sensitive to the orientation of **M** rather than to magnetic anisotropies. Here, we used SQUID magnetometry to record the projection m of the total magnetic moment **m** onto the direction of the external magnetic field **H**.

In a first series of experiments, we recorded m as a function of the external magnetic field magnitude $\mu_0 H$ at fixed orientations of **H** and fixed voltages V_p at $T = 300\,\text{K}$. Figure 4(a) shows $M = m/V$ measured with $\mathbf{H} \| \hat{\mathbf{y}}$ as a function of the external magnetic field strength at constant voltage $V_p = +30\,\text{V}$ (full circles) and $V_p = -30\,\text{V}$ (open triangles). The Ni film shows a rectangular $M(H)$ loop for $V_p = -30\,\text{V}$, while for $V_p = +30\,\text{V}$ the remanent magnetization is lowered by a factor of approximately three. According to, e.g. Morrish [30], the rectangular loop for $V_p = -30\,\text{V}$ indicates a magnetically easy axis, while the smooth, s-shaped loop for $V_p = +30\,\text{V}$ indicates a magnetically harder axis. Thus figure 4(a) shows that the $\hat{\mathbf{y}}$-direction is magnetically *easier* for $V_p = -30\,\text{V}$ and *harder* for $V_p = +30\,\text{V}$—as expected from the FMR experiments. Changing the orientation of **H** to $\mathbf{H} \| \hat{\mathbf{x}}$ yields the $M(H)$-loops shown in figure 4(b). Following the same line of argument we can conclude that the $\hat{\mathbf{x}}$-direction is magnetically *easier* for $V_p = +30\,\text{V}$ and *harder* for $V_p = -30\,\text{V}$. Altogether these results show that we observe an in-plane anisotropy, the easy axis of which is parallel to $\hat{\mathbf{y}}$ for $V_p = -30\,\text{V}$ and parallel to $\hat{\mathbf{x}}$ for $V_p = +30\,\text{V}$. These observations are fully consistent with the FMR results, and corroborate the simple model shown in figure 1.

Before discussing further experimental magnetometry results, we note that the free energy minima shown in figure 1(c) and (e) as well as the in-plane resonance fields in figure 3(a) are degenerate by $180°$. This degeneracy may lead to demagnetization due to domain formation if the polarity of V_p is repeatedly inverted as there are always two energetically equally favourable
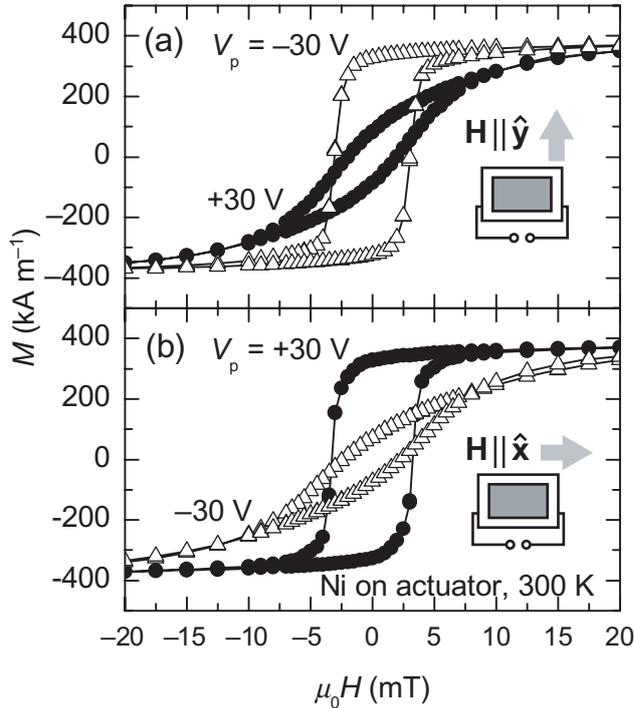
Figure 4. (a) $M(H)$-loops recorded with $\mathbf{H} \| \hat{\mathbf{y}}$ show a higher remanent magnetization for $V_p = -30\,\text{V}$ than for $V_p = +30\,\text{V}$, thus the $\hat{\mathbf{y}}$-axis is magnetically easier for $V_p = -30\,\text{V}$ than for $V_p = +30\,\text{V}$. (b) The $\hat{\mathbf{x}}$-axis is magnetically easier for $V_p = +30\,\text{V}$ than for $V_p = -30\,\text{V}$.

but opposite directions of $\mathbf{M}$. Thus, to achieve a reversible control of $\mathbf{M}$ orientation, the degeneracy of F_{tot} needs to be lifted. This can be achieved if a unidirectional anisotropy is superimposed on the uniaxial anisotropy. Regarding F_{tot} in equation (1), only F_{stat} possesses the desirable unidirectional anisotropy. Hence, a small but finite external magnetic field $\mathbf{H} \neq 0$ can be used to lift the 180° degeneracy. This approach works for all $\mathbf{H}$ orientations, except for $\mathbf{H}$ exactly parallel to $\hat{\mathbf{x}}$ or $\hat{\mathbf{y}}$. For $\mathbf{H} \| \hat{\mathbf{x}}$ (with $H > 0$), the easy axis parallel to $\hat{\mathbf{x}}$ in figure 1(c) is replaced by an easier positive $\hat{\mathbf{x}}$-direction and a harder negative $\hat{\mathbf{x}}$-direction, thus the degeneracy is lifted for $V_p > 0$. However, for $V_p < 0$ [cf figure 1(e)] a magnetic field $\mathbf{H} \| \hat{\mathbf{x}}$ is orthogonal to the easy axis which thus remains degenerate. The same consideration holds for $\mathbf{H} \| \hat{\mathbf{y}}$ where we expect degenerate free energy minima for $V_p > 0$ and a preferred $\mathbf{M}$ orientation for $V_p < 0$. However, in experiment it is essentially impossible to orient $\mathbf{H}$ *exactly* along $\hat{\mathbf{x}}$ or $\hat{\mathbf{y}}$; any small misorientation between $\mathbf{H}$ and $\hat{\mathbf{x}}$ or $\hat{\mathbf{y}}$ is sufficient to lift the degeneracy.

We now turn to the experimental measurement of the voltage control of $\mathbf{M}$ orientation. To show that $\mathbf{M}$ can be rotated by varying V_p alone, we change V_p at constant external magnetic bias field $\mathbf{H}$. As SQUID magnetometry is limited to recording the projection of $\mathbf{M}$ on the direction of the external magnetic field $\mathbf{H}$, it is important to choose appropriate $\mathbf{H}$ orientations in the experiments. As evident from figures 1 and 4, $\mathbf{H} \| \hat{\mathbf{x}}$ and $\mathbf{H} \| \hat{\mathbf{y}}$ are the most interesting orientations of the external magnetic field $\mathbf{H}$. In view of the circumstance discussed in the previous paragraph, we applied $\mathbf{H}$ to within 1° of $\hat{\mathbf{x}}$ or $\hat{\mathbf{y}}$, respectively. We still refer to these orientations of $\mathbf{H}$ as $\mathbf{H} \| \hat{\mathbf{x}}$ and $\mathbf{H} \| \hat{\mathbf{y}}$ for simplicity, but take into account a misalignment of 1° in the calculations.

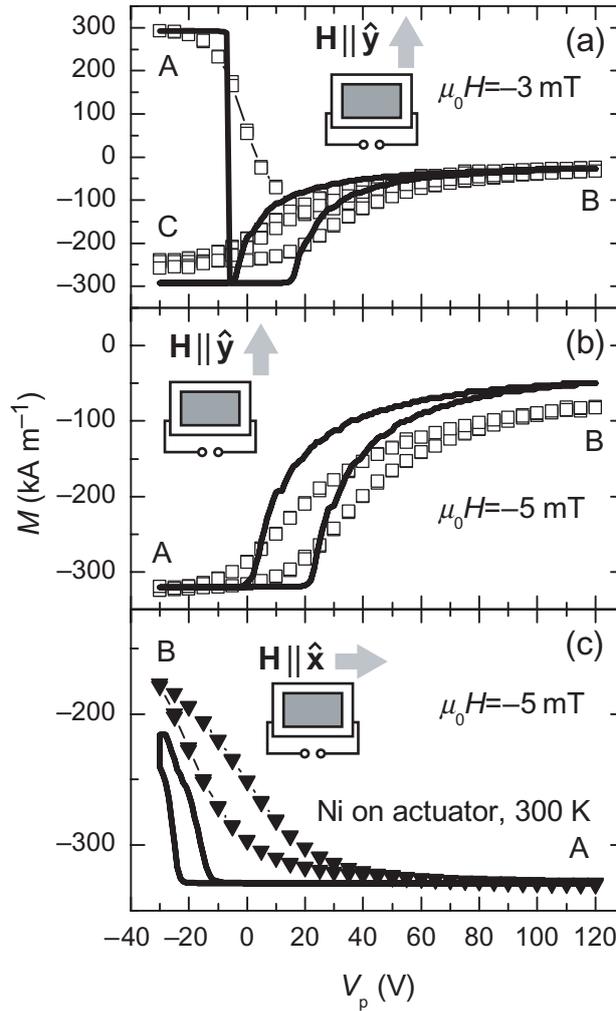**Figure 5.** SQUID $M(V_p)$-loops show the projection M of the magnetization **M** onto the direction of the applied magnetic field **H** as a function of V_p. The symbols represent the experimental data and the lines show the simulation of M resulting from a minimization of F_{tot} [equation (1)], with ε_2 determined using a strain gauge to explicitly take into account the actuator hysteresis. (a) For $\mathbf{H} \| \hat{\mathbf{y}}$ with $\mu_0 H = -3$ mT, **M** exhibits an *irreversible* rotation from A to B followed by a *reversible* rotation from B to C. (b) and (c) For $\mathbf{H} \| \hat{\mathbf{y}}$ and $\mathbf{H} \| \hat{\mathbf{x}}$ with $\mu_0 H = -5$ mT, **M** exhibits a *reversible* rotation from A to B and back to A.

As the experimental results and the corresponding simulations will show, this slight misalignment is sufficient to lift the degeneracy in the free energy regardless of V_p.

Recording M as a function of V_p for two complete voltage cycles $-30\,\mathrm{V} \leqslant V_p \leqslant +120\,\mathrm{V}$ with $\mathbf{H} \| \hat{\mathbf{y}}$ and $\mu_0 H = -3$ mT yields the data points shown in figure 5(a). Since $\mathbf{H} \| \hat{\mathbf{y}}$, M is the projection of **M** to the $\hat{\mathbf{y}}$-direction in the experiment. Prior to the first voltage sweep starting at point A, the voltage was set to $V_p = -30$ V and the sample was magnetized to a single domain state by applying $\mu_0 H = +7$ T along $\hat{\mathbf{y}}$ which is the easy axis for $V_p = -30$ V. The magnetic field was then swept to $\mu_0 H = -3$ mT which is close to but still below the coercive field of

the rectangular loops [cf figure 4] and the acquisition of the $M(V_p)$ data was started. The fact that M is positive at first (starting from point A), while the field is applied along the negative $\hat{\mathbf{y}}$-direction, shows that $\mathbf{M}$ and $\mathbf{H}$ are essentially antiparallel at first. Upon increasing V_p in steps of $+5\,$V to $V_p = +120\,$V (point B), M vanishes, which indicates an orthogonal orientation of $\mathbf{M}$ and $\mathbf{H}$. Upon reducing V_p to its initial value of $-30\,$V, M becomes negative (point C), evidencing a parallel orientation of $\mathbf{M}$ and $\mathbf{H}$. The V_p cycle was then repeated once more, with M now reversibly varying between its negative value at point C and zero at B. Hence the evolution of M is qualitatively different in the first and in the second V_p cycle, with an *irreversible* $\mathbf{M}$ rotation in the first cycle and a *reversible* $\mathbf{M}$ rotation in the second cycle. This behaviour is expected from the magnetic free energy [cf equation (1)] as the preparation (point A) yields $\mathbf{M}$ in a metastable state ($\mathbf{M}$ antiparallel to $\mathbf{H}$).

After a renewed preparation with $\mu_0 H = +7\,$T at $V_p = -30\,$V, we repeated the experiment with the external magnetic field $\mathbf{H}\|\hat{\mathbf{y}}$ but with a slightly larger magnitude $\mu_0 H = -5\,$mT and again recorded M for a complete voltage cycle. The magnetic field magnitude of $\mu_0 H = -5\,$mT was chosen as it exceeds the coercive field [cf figure 4] while keeping the influence of the Zeemann term in equation (1) on the total magnetic anisotropy comparable to the influence of the strain-induced anisotropies [cf equation (9)]. The experimental data are shown by the symbols in figure 5(b). Here, a parallel orientation of $\mathbf{M}$ and $\mathbf{H}$ is already observed at point A ($V_p = -30\,$V) and $\mathbf{M}$ rotates reversibly by approximately $70°$ towards point B ($V_p = +120\,$V) and back when V_p is reduced to $-30\,$V again (point A).

To complete the picture, we repeated the $M(V_p)$ experiment again, but now applied $\mathbf{H}\|\hat{\mathbf{x}}$. The magnetic preparation with $\mu_0 H = 7\,$T was now performed at $V_p = +120\,$V to ensure that the preparation field was again applied along an easy axis. The data recorded subsequently at $\mu_0 H = -5\,$mT [cf figure 5(c)] show a reversible rotation of $\mathbf{M}$ by approximately $60°$ between points A, B ($V_p = -30\,$V) and back to A.

To quantitatively simulate the evolution of M with V_p depicted in figure 5, we again took advantage of the fact that the free energy of the Ni film is known from the FMR experiments. To account for the hysteresis of the actuator expansion which is responsible for hysteresis in the $M(V_p)$ loops in figure 5, we hereby used ε_2 as measured using a Vishay general purpose strain gauge in the voltage range of $-30\,$V $\leqslant V_p \leqslant +120\,$V. The ε_2 data thus obtained are in accordance with the actuator data sheet. Using $\varepsilon_2(V_p)$ as well as the material constants given above we obtained in-plane free energy contours for each voltage V_p. Figure 6 exemplarily shows such free energy contours at the voltages depicted by the capital letters in figure 5. To clearly visualize the effect of $\mathbf{H}$ misalignment with respect to the sample coordinate system on F_{tot}, the plots in figure 6 were calculated assuming a misalignment in the in-plane orientation of the external magnetic field θ of $10°$, so that $\theta = 10°$ for $\mathbf{H}\|\hat{\mathbf{y}}$ and $\theta = 100°$ for $\mathbf{H}\|\hat{\mathbf{x}}$. Figure 6 clearly shows that under these conditions the local minima of F_{tot} are non-degenerate for $V_p = -30\,$V and $V_p = +120\,$V.

To determine the orientation of $\mathbf{M}$, we traced the minimum of the total free energy F_{tot} as a function of V_p. This was done by minimizing equation (1) with respect to the in-plane orientation Θ of $\mathbf{M}$, whilst assuming that $\Phi = 90°$ due to the strong shape anisotropy.

To simulate the experimental $M(V_p)$-loops [cf figure 5], we assume a more realistic misalignment of $1°$ in θ and numerically minimize $F_{tot}(\Theta)$ as a function of V_p. For this, we set the initial value of Θ antiparallel to the external magnetic field for $\mu_0 H = -3\,$mT and parallel to the external magnetic field for $\mu_0 H = -5\,$mT. Minimizing $F_{tot}(\Theta)$ determines the $\mathbf{M}$ orientation which we project onto the $\hat{\mathbf{y}}$- or $\hat{\mathbf{x}}$-axis to yield M. For this, the magnitude of $\mathbf{M}$ is
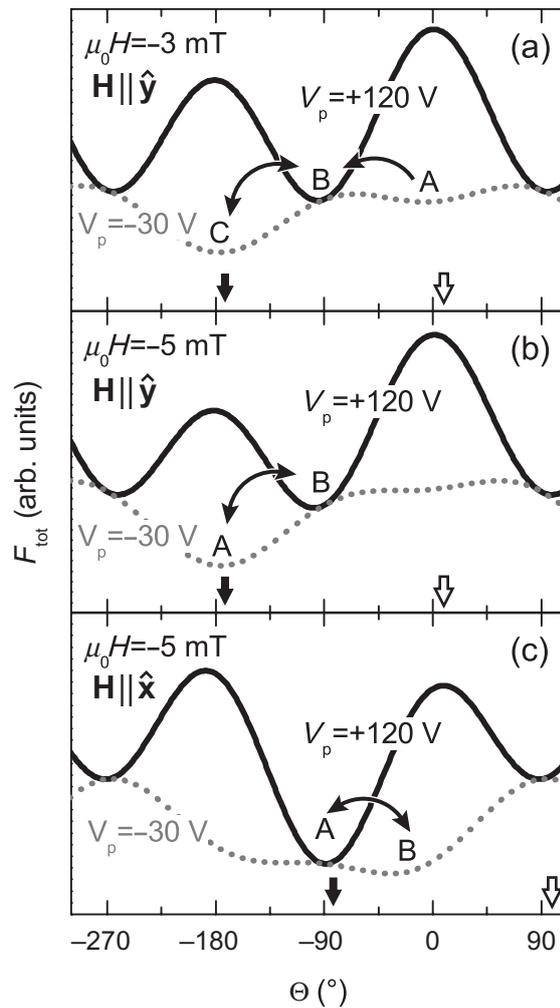
Figure 6. Calculated free energy contours in the film plane at the points of the $M(V_{\mathrm{p}})$-loop depicted by capital letters in figure 5 (solid lines: $V_{\mathrm{p}} = +120\,\mathrm{V}$, dotted lines: $V_{\mathrm{p}} = -30\,\mathrm{V}$). To clarify the lifting of the free energy degeneracy by the magnetic field, an angle of $10°$ between the magnetic field and the $\hat{\mathbf{x}}$- or $\hat{\mathbf{y}}$-axis was assumed. The open downward-oriented arrows depict the orientation of $\mathbf{H}$ during the field preparation at $7\,\mathrm{T}$ and the closed downward-oriented arrows depict the orientation of $\mathbf{H}$ during the actual measurement. Capital letters indicate the equilibrium $\mathbf{M}$ orientation at the corresponding positions in figure 5. (a) Subsequent to the field preparation at $-30\,\mathrm{V}$, $\mathbf{M}$ resides in a *local* minimum of F_{tot} (point A) at $\mu_0 H = -3\,\mathrm{mT}$ and rotates to the *global* minimum of F_{tot} at (point B) as V_{p} is increased to $V_{\mathrm{p}} = +120\,\mathrm{V}$. Sweeping the voltage from $+120\,\mathrm{V}$ to $-30\,\mathrm{V}$ now results in $\mathbf{M}$ following the *global* minimum of F_{tot}. (b) and (c) For $\mu_0 H = -5\,\mathrm{mT}$, $\mathbf{M}$ follows the *global* minimum of F_{tot} as V_{p} is changed.

chosen to give a good fit to the experimental data at points A and is assumed to remain constant independent of V_{p}.

The resulting simulations of M are shown by the solid lines in figure 5. The simulation yields the experimentally observed *irreversible* $\mathbf{M}$ rotation during the first voltage sweep in

figure 5(a) as well as the *reversible* **M** rotations in the second voltage sweep in figure 5(a) and in figures 5(b) and (c). The simulated total swing of M is in excellent agreement with the experimental results for $\mathbf{H} \| \hat{\mathbf{y}}$ and in good agreement for $\mathbf{H} \| \hat{\mathbf{x}}$. The fact that the experimental results exhibit a more rounded shape than the simulation is attributed to domain formation during the magnetization reorientation, which is neglected in the simulation.

Taken together, the free energy density of equation (1) with the contributions quantitatively determined from FMR and our simple simulation of $M(V_p)$ yield excellent agreement with experiment. In particular, we would like to emphasize that for the experiment and the simulation the application of V_p leads to a *rotation* of **M** and not to a decay into domains. This is evident from the fact that in figures 5(a) and (b), a large projection of **M** onto $\hat{\mathbf{y}}$ is accompanied by a small projection onto $\hat{\mathbf{x}}$ and vice versa. Combining FMR and SQUID magnetometry, we thus have unambiguously and quantitatively demonstrated that **M** can be rotated reversibly by about $70°$ at room temperature solely via the application of appropriate voltages V_p.

6. Conclusions and outlook

In conclusion, we have investigated magnetoelastic coupling effects in Ni/piezoactuator hybrids, using both FMR and SQUID magnetometry. The FMR measurements show that the in-plane anisotropy of Ni/piezoactuator hybrids can be inverted if the polarity of the voltage applied to the actuator is changed. Thus, we do not only observe a magnetoelastic contribution to magnetic anisotropy, as one might expect considering the properties of the constituents. Rather, in the hybrid structure, the magnetoelastic coupling is strong enough to dominate over all other contributions to the in-plane magnetic free energy. The magnetometry experiments corroborate this result and furthermore show that it is possible to irreversibly or reversibly rotate **M** solely by changing V_p. For an *irreversible* $M(V_p)$ rotation, an appropriate preparation of **M** using a magnetic field sweep is necessary—i.e. **M** must be aligned in a local free energy minimum. It then can be rotated out of this minimum by changing V_p and the corresponding **M** orientation change can amount to up to $180°$. However, this voltage control of **M** is irreversible in the sense that **M** cannot be brought back into the original orientation by changing V_p alone. Rather, a second appropriate magnetic field sweep is required to align **M** into its original orientation. In contrast, the *reversible* $M(V_p)$ reorientation requires a preparation of **M** only once. In this case, **M** is oriented along a global free energy minimum, and can be rotated within up to $70°$ ($90°$ in the ideal case) at will by applying an appropriate V_p. The $M(V_p)$-loops simulated by minimizing the single-domain free energy [equation (1)] in a Stoner–Wohlfarth type of approach are in excellent agreement with experiment, showing that the **M** orientation can be accurately calculated from the free energy determined from FMR as a function of external magnetic and/or electric field strengths. Furthermore, we would like to point out that the hysteretic expansion/contraction of the actuator visible as a hysteresis in $M(V_p)$ [cf figure 5] in particular also leads to distinctly different $M(V_p = 0)$, depending on the V_p history. Thus, our data also demonstrate that a remanent **M** control is possible in our ferromagnetic thin film/piezoelectric actuator hybrids. Finally, we note that an electric field control of magnetization orientation via the elastic channel should be possible in any material or hybrid system, given that the magnetoelastic contribution to the magnetic free energy dominates in the plane of interest. In our opinion, this approach thus can be implemented and exploited in a variety of existing spintronic devices, e.g. to control the magnetization orientation in individual magnetic random

access memory bits. Additionally, the application of an ac electric field to the actuator will generate a time-dependent strain in the ferromagnet, opening an avenue for the control and investigation of magnetization dynamics.

Acknowledgments

References

[1] Slonczewski J C 1996 *J. Magn. Magn. Mater.* **159** L1
[2] Berger L 1996 *Phys. Rev.* B **54** 9353
[3] Tsoi M, Jansen A G M, Bass J, Chiang W-C, Seck M, Tsoi V and Wyder P 1998 *Phys. Rev. Lett.* **80** 4281
[4] Zhang S, Levy P M and Fert A 2002 *Phys. Rev. Lett.* **88** 236601
[5] Spaldin N A and Fiebig M 2005 *Science* **309** 391
[6] Eerenstein W, Mathur N D and Scott J F 2006 *Nature* **442** 759
[7] Fiebig M, Lottermoser T, Lonkai T, Goltsev A and Pisarev R 2005 *J. Magn. Magn. Mater.* **290–291** 883
[8] Ramesh R and Spaldin N A 2007 *Nat. Mater.* **6** 21
[9] Lottermoser T, Lonkai T, Amann U, Hohlwein D, Ihringer J and Fiebig M 2004 *Nature* **430** 541
[10] Gajek M, Bibes M, Fusil S, Bouzehouane K, Fontcuberta J, Barthelemy A and Fert A 2007 *Nat. Mater.* **6** 296
[11] Chu Y-H *et al* 2008 *Nat. Mater.* **7** 478
[12] Zhao T *et al* 2006 *Nat. Mater.* **5** 823
[13] Stolichnov I, Riester S W E, Trodahl H J, Setter N, Rushforth A W, Edmonds K W, Campion R P, Foxon C T, Gallagher B L and Jungwirth T 2008 *Nat. Mater.* **7** 464
[14] Binek C and Doudin B 2005 *J. Phys.: Condens. Matter* **17** L39
[15] Bootsmann M-T, Dokupil S, Quandt E, Ivanov T, Abedinov N and Lohndorf M 2005 *IEEE Trans. Magn.* **41** 3505
[16] Wan J G, Liu J-M, Wang G H and Nan C W 2006 *Appl. Phys. Lett.* **88** 182502
[17] Dörr K and Thiele C 2006 *Phys. Status Solidi* b **243** 21
[18] Goennenwein S T B, Althammer M, Bihler C, Brandlmaier A, Geprägs S, Opel M, Schoch W, Limmer W, Gross R and Brandt M S 2008 *Phys. Status Solidi (RRL)* **2** 96
[19] Brandlmaier A *et al* 2008 *Phys. Rev.* B **77** 104445
[20] Bihler C *et al* 2008 *Phys. Rev.* B **78** 045203
[21] Overby M, Chernyshov A, Rokhinson L P, Liu X and Furdyna J K 2008 *Appl. Phys. Lett.* **92** 192501
[22] Ranieri E D *et al* 2008 *New J. Phys.* **10** 065003
[23] Wang D, Nordman C, Qian Z, Daughton J M and Myers J 2005 *J. Appl. Phys.* **97** 10C906
[24] Stoner E C and Wohlfarth E P 1948 *Phil. Trans. R. Soc.* A **240** 599
[25] Piezomechanik GmbH, Munich 2006 *Low Voltage Co-Fired Multilayer Stacks, Rings and Chips for Actuation* Model Pst 150/2x3/5, low temperature
[26] Kittel C 1995 *Introduction to Solid State Physics* 7th edn (New York: Wiley)
[27] Danan H, Herr A and Meyer A J P 1968 *J. Appl. Phys.* **39** 669
[28] Chikazumi S 1997 *Physics of Ferromagnetism, The International Series of Monographs on Physics* 2nd edn (New York: Oxford Science Publications)
[29] Lee E W 1955 *Rep. Prog. Phys.* **18** 184

IOP Institute of Physics Φ DEUTSCHE PHYSIKALISCHE GESELLSCHAFT

[30] Morrish A H 2001 *The Physical Principles of Magnetism* 1st edn (New York: IEEE Press)
[31] Nye J F 1985 *Physical Properties of Crystals* (Oxford: Oxford University Press)
[32] Smit J and Wijn H P J 1954 *Adv. Electron. Electron Phys.* **6** 70
[33] Smit J and Beljers H G 1955 *Philips Res. Rep.* **10** 113
[34] Suhl H 1955 *Phys. Rev.* **97** 555
[35] Poole C P 1996 *Electron Spin Resonance* 2nd edn (New York: Dover)
[36] Meyer A J P and Asch G 1961 *J. Appl. Phys.* **32** 330